Quaternary Science Reviews 313 (2023) 108197

Contents lists available at ScienceDirect

Quaternary Science Reviews

journal homepage: www.elsevier.com/locate/quascirev

New datings and elevations of a fossil reef in Lembetabe, southwest Madagascar: eustatic and tectonic implications

J. Weil-Accardo [a, *], P. Boyden [b], A. Rovere [b, c], N. Godeau [a], N. Jaosedy [d], A. Guihou [a], M. Humblet [e], M.N. Rajaonarivelo [d], J. Austermann [f], P. Deschamps [a]

[a] Aix Marseille University, CNRS, IRD, INRAE, College de France, CEREGE, Aix-en-Provence, France
[b] MARUM, University of Bremen, Germany
[c] Department of Environmental Sciences, Informatics, and Statistics, Ca'Foscari University of Venice, Venice, Italy
[d] CNRO, Hell-Ville, Nosy Be, Madagascar
[e] Department of Earth and Planetary Sciences, Nagoya University, Nagoya, Japan
[f] Department of Earth and Environmental Sciences, Columbia University, Palisades, USA

ARTICLE INFO

Article history:
Received 25 November 2022
Received in revised form
3 June 2023
Accepted 15 June 2023
Available online 06 July 2023

Handling Editor: I Hendy

Keywords:
Last interglacial
Sea-level changes
West Indian ocean
Geochronology
Glacial isostatic adjustment modeling

ABSTRACT

The study of geological sea-level proxies formed during previous interglacials is a common approach to assess how global sea level will evolve under warmer climate conditions. Over the last decades, technical advancements in both survey and geochronology have allowed improving our knowledge of past sea-level highstands. This is of prime importance to refine our understanding of processes contributing to sea-level changes, and ultimately to improve both local and global sea-level projections. Last Interglacial sea-level proxies in the Western Indian Ocean (and more specifically the island nation of Madagascar), have been less investigated than in other intertropical oceans over the last decades. As a result, paleo sea-level data in this region are less abundant and less precise than elsewhere. Here, we report the results of two field campaigns aimed at studying the site of Lembetabe, southwest Madagascar, where a fossil reef was first described by the researcher René Battistini more than 50 years ago. We estimate paleo relative sea level history in space and time from 15 new U-series ages from a fossil reef platform mapped with differential GNSS and drone photogrammetry. Our data suggest that, between 129 ka and 115 ka, paleo relative sea level at this location was about 3.4 ± 1.4 m above modern. Once corrected for glacial isostatic adjustment, we find that paleo global mean sea level did not exceed 3 m above modern. Only slight crustal subsidence would reconcile the peak Last Interglacial sea level measured at Lembetabe with the 5 −10 m range reported in the literature.

1. Introduction

Global mean sea level (GMSL) has been rising for the last 150 years (Church et al., 2013), and will continue to rise as global temperatures increase unabated (Pörtner et al., 2019). Until recently, the main contributor to GMSL was mainly due to the thermosteric expansion of seawater (e.g. Church et al., 2013). In the last decade, melting of polar ice caps started to dominate the sea-level signal (e.g. Shepherd et al., 2012). In this context, understanding the potential upper bounds of polar ice melting in warmer climates is essential to gauge how much and how fast sea level may rise in the future. For this reason, geological sea-level proxies (or sea-level indicators, i.e., geological features deposited or formed by past sea levels) are used to constrain past sea-level changes and, in turn, assess ice melting in past warm periods (Chappell, 1974; Shackleton and et Matthews, 1977; Bard et al., 1990; Blanchon et al., 2009; O'Leary et al., 2013). Any paleo sea-level proxy requires that certain conditions on survey, geological interpretation, and dating are met (Shennan et al., 2015). First, elevation of the stratigraphic elements closely related to paleo sea level must be measured as accurately as possible and referenced to a known datum. This is becoming simpler with the decrease in price and increase in the usability of differential Global Navigation Satellite System (dGNSS) devices. Then, geomorphological, sedimentological and/or taxonomical properties must be understood in detail, and related to a modern analog to understand the position of the paleo sea level

* Corresponding author.
E-mail address: weil@cerege.fr (J. Weil-Accardo).

https://doi.org/10.1016/j.quascirev.2023.108197
0277-3791/

with respect to the elevation of the sea-level indicator (Rovere et al., 2016a; Hibbert et al., 2016). A sea-level proxy must also be attributed to an absolute age with radiometric dating methods. For fossil reefs, the development of U-series dating (e.g. Ivanovich et Harmon, 1992) has allowed the dating of Pleistocene fossil reefs globally (e.g. Veeh, 1966). Successive improvements (e.g. Edwards et al., 1987; Edwards, 1988; Cheng et al., 2013; Chiang et al., 2019), namely the use of thermal ionization mass spectrometer (TIMS) and (more recently) of multi-collector inductively-coupled plasma mass spectrometer (MC-ICPMS) allow to measure fossil reef ages with error bars of 0.5–2 kyr (2σ) (e.g. Kerans et al., 2019).

The second factor that needs to be accounted for when using any sea-level indicator to reconstruct past GMSL changes is that, over time, the Earth's crust has been subject to vertical motions, that must be either added or subtracted from the current elevation of the indicator before paleo GMSL is calculated. Vertical land motions may be due to tectonics (e.g., in areas close to active tectonic margins such as New Guinea, Chappell, 1974) or subsidence related to sediment loading (Simms et al., 2013) or sediment compaction. Austermann et al. (2017) also pointed out that, even at passive margins, mantle dynamic topography can cause vertical land movements of several meters since the LIG. Furthermore, as water mass shifts between ice and ocean reservoirs over glacial-interglacial cycles, the loading and unloading of mass causes deformation of the Earth's surface. This deformation generates a disequilibrium that is then compensated by glacial isostatic adjustment (GIA) due to the viscous behavior of the mantle (e.g. Lambeck and et Chappell, 2001) in response to ice sheet melting and regrowth. Until the elevation of a sea-level indicator (e.g., a fossil reef) is corrected for these post-depositional vertical movements, it is commonly referred to as a relative sea level (RSL), as opposed to GMSL, or "eustatic" (Rovere et al., 2016b), that is the sum of barystatic and thermosteric sea-level changes (sensu Gregory et al., 2019).

One time period that is widely studied to understand the sensitivity of polar ice to slightly warmer climatic conditions is the Last Interglacial (LIG, Marine Isotopic Stage 5e, 115–129 ka). During the LIG, global atmospheric temperatures were estimated 0.5–1.5 °C warmer than in 1850–1900 (Fox-Kemper et al., 2021) and GMSL a few meters above pre-industrial (Dutton et al., 2015a; Gulev et al., 2021; Dyer et al., 2021).

To gauge the maximum level attained by GMSL during the LIG, several studies surveyed and dated LIG fossil sea-level indicators, then correct for post-depositional vertical land motions using geodynamic models or estimates of tectonic uplift or subsidence using from independent constraints. There has been a convergence of results suggesting that the maximum elevation attained by GMSL during the LIG was 5–10 m above the pre-industrial (Gulev et al., 2021). However, recent estimates from sea-level indicators in the Bahamas seem to imply a lower estimate, ranging between 1.2 and 5.3 m (Dyer et al., 2021).

Among the key issues preventing the convergence of LIG sea-level estimates is that, despite thousands of sites globally that have preserved LIG sea-level indicators, only few have been measured and dated with state-of-the-art techniques, enabling more precise paleo RSL reconstructions (Rovere et al., 2022). Higher accuracy in defining the distribution in space and time of RSL indicators is of prime importance to evaluate the possibility of meter-scale sea-level fluctuations within the LIG highstand, that would imply periods of melting and regrowth of ice caps (e.g. Blanchon et al., 2009; Kopp et al., 2013; Barlow et al., 2018; Polyak et al., 2018; Rohling et al., 2019).

In this general context, there is a comparatively greater abundance of studies focused on LIG fossil reefs in the Pacific and Atlantic oceans (as evidenced by global compilations by Hibbert et al., 2016; Rovere et al., 2022) when compared to the Western Indian Ocean (for which a recent compilation from Boyden et al., 2021). More specifically, in Madagascar the study of Pleistocene sea-level changes was pioneered in the north of the island by Lemoine (1906). This work was followed, nearly 50 years later, by a first detailed study on coastal geomorphology from Diego Suarez to Analalava (Guilcher, 1954). The French geoscientist René Battisini led several works throughout the mid-60's to late 70's on past sea-level indicators in several areas of Madagascar, as well as at a few sites in Tanzania, Kenya, Seychelles archipelago and Eparses islands (Battistini, 1965a,b, 1966, 1969; Battistini et al., 1970; Battistini, 1970a,b, 1972; Battistini et Cremers, 1972; Battistini et al., 1976; Battistini, 1977; Battistini et Jouannic, 1979). Since these early pioneering works, the only study conducted on Malagasy Pleistocene sea-level indicators was recently published by Stephenson et al. (2019) on the northern tip of the island.

At the time of pioneering Malagasian works mentioned above, elevations were measured at best with an optical level, and the referencing to the tidal level was often not implemented rigorously. Concerning age determination, alpha-counting techniques were used to measure U–Th disequilibrium for samples older than 50 kyr. Added to technical limitations (long analysis duration, large sample size), the 2σ accuracy in age was about 10 kyr for an age ranging between 70 ka and 150 ka (e.g. Edwards et al., 2003). Today, we are able to reach centimetric accuracy with dGPS surveys (Rovere et al., 2016a), and data can be better referenced to mean sea level (MSL) thanks to the wide availability of local geoids, benchmarks from tide gauges, or easily deployable water level loggers. Further, with the development of mass spectrometry and the emergence of MC-ICPMS, we can now routinely reach uncertainties of only 0.5 kyr (2σ) for a sample of about 100 kyr old (e.g. Kerans et al., 2019).

Recently, Boyden et al. (2022) revisited a site on the southwest coast of Madagascar, close to a town called Lembetabe. The site is characterized by an emerged reef of Last Interglacial age, that was first reported by Battistini (1965a) (Fig. S1 in Supplementary Material), and initially dated to 85 ± 4–5 ka with the U–Th alpha-counting method (Battistini et al., 1976; Battistini, 1977). Based on coastal stratigraphy analysis, Boyden et al. (2022) show that the fossil reef at Lembetabe is representative of a shallow-water regressive sequence, spanning in age from the beginning of MIS 5e to the end of it. The entire MIS 5e reef complex sits on top of an older reef, likely of MIS 11 age.

Here, we present 16 new U-series ages on corals sampled from the Lembetabe section, each measured with dGNSS. This mostly new data set, added to the ages already presented by Boyden et al. (2022), make this fossil reef section one of the best dated globally. We then use the descriptions of the reef facies by our companion paper (Boyden et al., 2022) and a new satellite-derived bathymetry of the modern lagoon in front of the village of Lembetabe to quantify the indicative meaning of the fossil reef, and ultimately calculate a paleo RSL curve for this area. We then correct our data with a suite of 576 GIA models with varying ice and earth models and discuss possible vertical land motions, in search for a best-matching Last Interglacial GMSL scenario.

2. Methodology

2.1. Site description

The Lembetabe site is located south of Toliara and about 11 km south of the town of Itampolo (Fig. 1 a-b). It belongs to the Mahafaly region (southwest of Madagascar) whose major tectonic feature is the NNW-SSE trending Toliara fault that separates the coastal plain from the eastward Mahafaly Plateau (Fig. 1 a-b). In this area, we

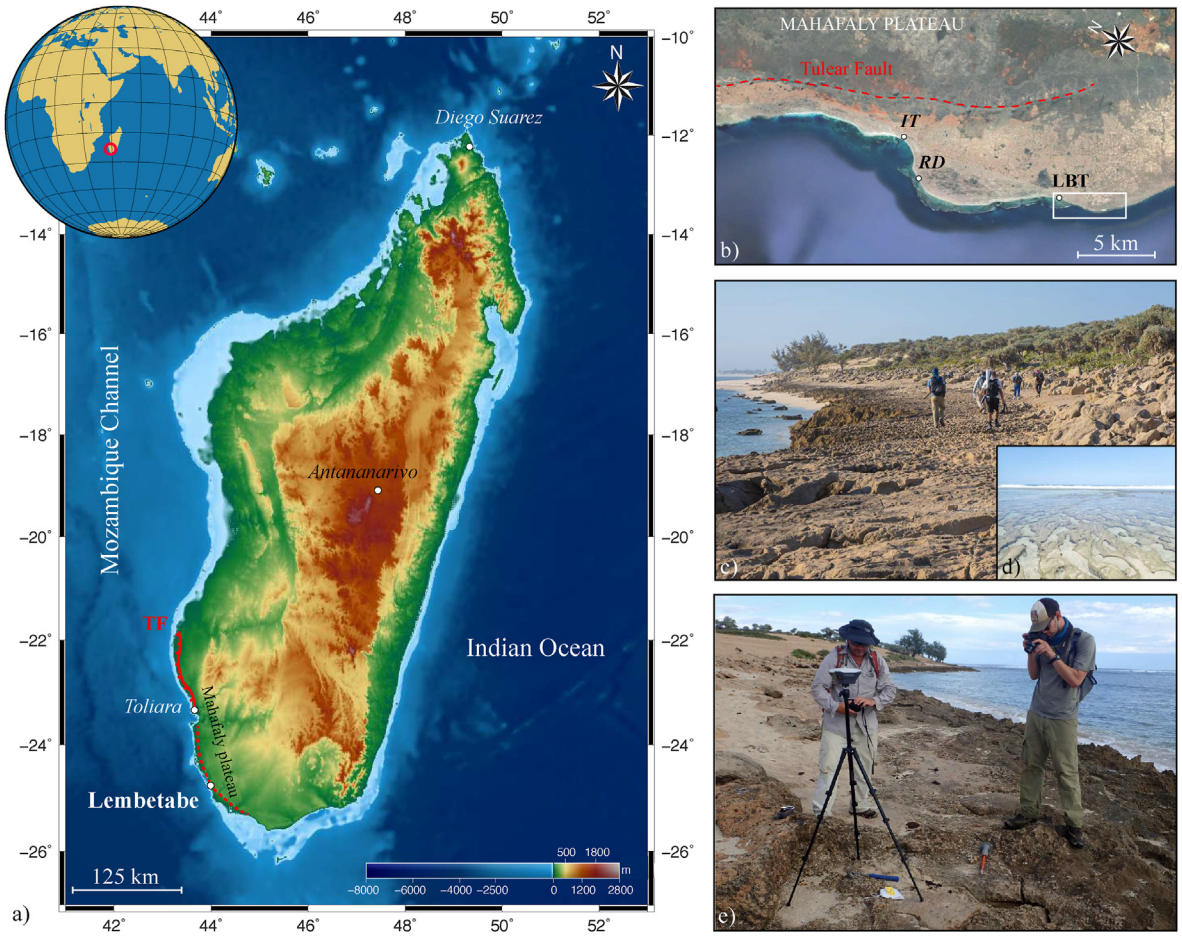

Fig. 1. Investigated area. a) Map of Madagascar with topography and bathymetry data (1 arc-minute global relief model) from ETOPO1 (https://www.ngdc.noaa.gov/mgg/global/global.html). White dots: main cities and location of the village of Lembetabe south of Toliara. Red line: assumed trace of the Toliara Fault (TF). b) Google Earth screenshot of the area investigated with location of the Toliara Fault (dashed red line) that might lower the SW coast located on the hanging wall of the normal fault. White rectangle: investigated area. LBT: Lembetabe, IT: Itampolo, RD: Raindrano. c) Field pictures of the marine terrace with the paleo abraded platform, the modern one (d), and the reef section (e) where fossil corals were measured and collected. Pictures of collected samples are given in Supplementary (Figs. S2 and S3). Additional field pictures of the paleo abraded platform and the modern one are given in Fig. 6.

studied an emerged fossil reef located close to the entrance of the Vezo fisherman village (24°47′15.52″S, 43°57′12.25″E, Fig. 1). The fossil reef extends over about 200 m from the village towards the south, and it is about 10 m wide across shore (Fig. 2). The fossil reef lies upon a broader terrace, of possible marine origin, stretching southward over about 12 km along the coast (Fig. 1 c). Acccording to tide predictions from the SHOM (Hydrographic and Oceanographic Department of the French Navy) for the Toliara tide gauge station, the tidal range is ranging between 1.5 and 2 m in average with more than 3 m of amplitude during equinox tides.

Within the emerged fossil reef, we observed numerous corals in growth position, with size (diameter) ranging between several tens of centimeters to about 2 m (Fig. 1 d and S2 and S3). The abundance of corals in a limited area, their upright position, and size for the larger ones suggest that most of these corals are *in situ*. As well, articulated bivalves, as *in situ* indicator were also noted on the reef section (Fig. S4). North of the reef section, there is no evidence of a former reef. To the south, we could not identify any more corals in growth position, but only fragments or other marine fossil organisms (marine mollusc shells and coral rubble), and terrestrial debris (terrestrial mollusc shells and pieces of ostrich eggshell). The fossil reef section is adjacent to the modern reef flat, whose width dramatically decreases southward from a maximal width of about 650 m in front of the fossil reef to a stable width of about 100 m towards the south (Fig. 1 b). On the modern reef flat, we identified massive *Porites* colonies, that have developed a microatoll morphology with their upward growth limited by annual lowest tide (e.g. Scoffin et al., 1978) (Fig. S5). At several locations we noted a relic flat surface of marine origin with paleo-furrows, that we interpret as a paleo shore platform (Fig. 1 c), similar to those observable within the modern intertidal area (Fig. 1 d). For a more comprehensive description of the coastal Pleistocene deposits in Lembetabe, the reader is referred to Boyden et al. (2022).

2.2. Field survey

To collect field data we used dGNSS, pressure transducers, single beam bathymetric sonars, and Unoccupied Aerial Vehicles (UAVs). Details on the data collection workflow are summarized hereafter, and described in full by Boyden et al. (2022).

A pair of Emlid REACH RS + single-band GNSS receivers in a Base-Rover configuration were used in order to obtain the most accurate vertical position of survey points along the paleo reef investigated in this study. Because of the remote nature of Lembetabe, the use of Real-Time Kinematic (RTK) corrections were not available and instead GNSS data was processed using a Precise Point

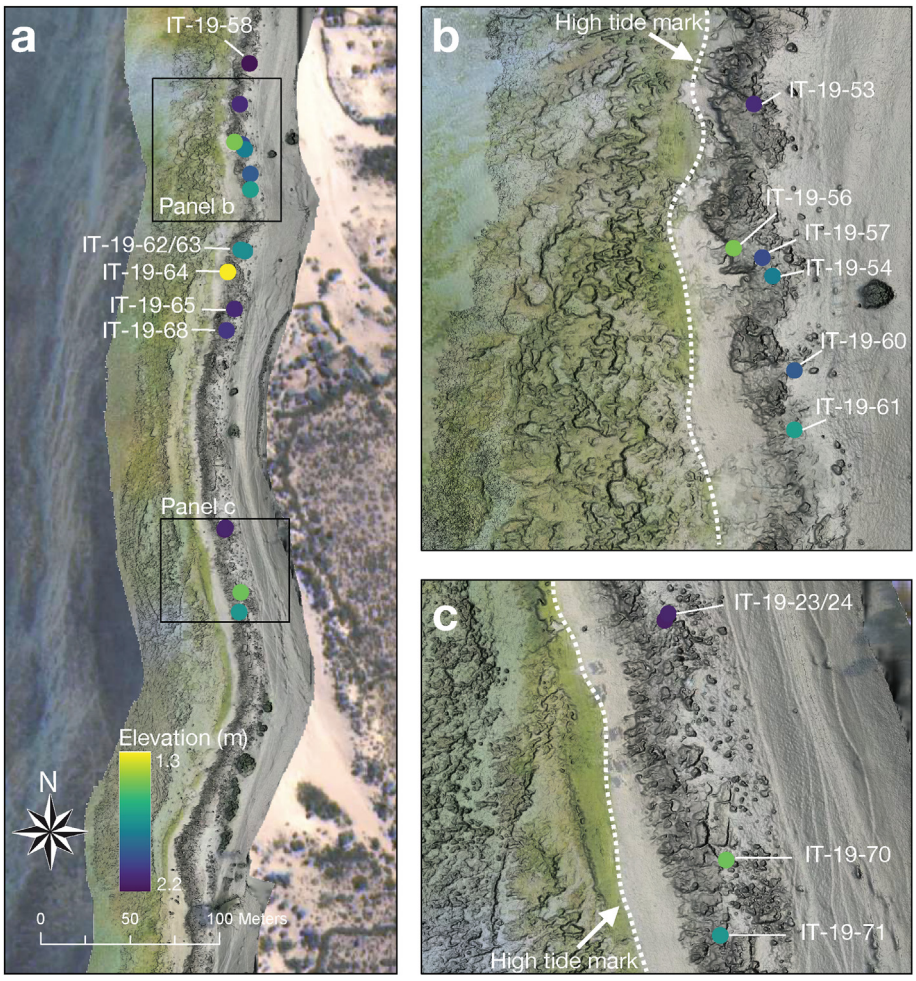

Fig. 2. Results of the drone survey (orthophoto and hillshade) of the fossil reef at Lembetabe, with elevations of samples reported in Table 2 and sample names given. a) entire scene; b) and c) detailed views. Background image from Worldview-2 (pansharpened), ©DigitalGlobe inc.

Positioning (PPP) workflow. This entails first processing the Base data online via the Canadian Spatial Reference System (CSRS) PPP tool provided by Natural Resources Canada (NRCan) then correcting the Rover data within the RTKLIB (v. 2.4.3) environment to the post-processed Base. Final elevations following this step are reported in ellipsoid height.

In order to correct the ellipsoid elevation (output of the dGNSS) to a known datum (e.g., MSL), chart datums or tidal benchmarks are often used. Again, because of the remote nature of the Lembetabe site, no chart datum exists and therefore a new datum needs to be established. To accomplish a reference to mean sea level, two INW PT2X Seametrics pressure transducers were deployed in tandem (onshore, to measure air pressure, and offshore to measure water levels) during the entirety of the field work (about 10 days). The position of each sensor was subsequently measured using the standard GNSS workflow (outlined above) and the resulting pressure data was then processed using Aqua4Plus. MSL was inferred from the resulting tidal stage and compared to the predicted tidal curve for Androka and Toliara to correct for any weather influence (see Boyden et al., 2022, for workflow details).

Commonly referred to as photogrammetry, the application of Structure from Motion/Multi-View Stereo (SfM/MVS) to reconstruct various geological settings is well established (e.g., Bistacchi et al., 2015; Casella et al., 2017; Bilmes et al., 2019). Utilizing the GNSS workflow outlined earlier, ground control points were distributed evenly along the paleo reef. Then, a DJI Mavic Pro UAV was flown at approximately 30 m altitude in a regular grid over the emergent reef at Lembetabe (see Boyden et al., 2022, for details). A total of 1111 photos were captured by the UAV with approximately 90% overlap. The captured photo sets were then processed using the commercial software Agisoft Metashape (v. 1.7.2 build 12070) to produce a final 3D orthomosaic and DEM of the reef sequence (see Boyden et al., 2022, for details).

In order to calculate the paleo waterdepth of the fossil reef at Lembetabe (and therefore derive a paleo RSL estimate at this location), we analyzed the mean depth distribution of the modern backreef directly offshore Lembetabe (considered as a modern analog of the fossil reef following the methodology of Rovere et al., 2016a). To do this, WorldView 2 (v. 28.4, May 2020) satellite imagery for the Lembetabe reef was processed using the SPEAR Relative Water Depth toolset within ENVI ® (https://www.l3harrisgeospatial.com/Software-Technology/ENVI) to generate a bathymetric DEM. This bathymetry was calibrated using single beam sonar soundings obtained with a Deeper Smart Sonar Pro ™ (www.deepersonar.com), a consumer-grade fishfinder. Each measured depth was corrected for the tidal variations and then converted to the MSL datum calculated by Boyden et al. (2022). The backreef/lagoon area was masked within QGIS (www.qgis.org) and the resulting bathymetry was extracted.

2.3. Coral sampling and U–Th dating with MC-ICPMS

We sampled 25 corals found *in situ* in growth position from the fossil reef at Lembetabe. The samples were chosen using the usual visual and audible criteria to distinguish between altered or preserved aragonite (e.g. Edwards et al., 2003).

Mineralogical analyses and U–Th dating were carried out at CEREGE. After visual examination with binocular microscope and prior to U–Th analysis, X-ray diffraction analyses were performed on all samples to identify any postmortem diagenetic alteration of their aragonite skeletons. Calcite content was estimated with the calibration equation obtained on the X'PERT PRO machine by Sepulcre et al. (2009). Only samples with less than 1% calcite were considered for U–Th dating. U–Th analyses were performed using a double ^{236}U–^{233}U–^{229}Th spike calibrated against an aliquot of the Harwell HU-1 uraninite standard originating from GEOTOP (see Deschamps et al., 2012, for details). U–Th ages were calculated using the half-lives provided by Cheng et al. (2013) for ^{230}Th (75,584 yr) and ^{234}U (245,620 yr). Details of the chemical procedure and analyses conducted on an MC-ICPMS NEPTUNE (following the procedure of Chiang et al., 2019) are given in Appendix.

2.4. Glacial isostatic adjustment models

To calculate the contribution of GIA to the modern elevation of LIG sea-level indicators, we use the same suite of models employed by Dyer et al. (2021). The models are based on the sea-level equation solved by Kendall et al. (2005), which accounts for the migration of shorelines and feedbacks into Earth's rotation axis. For sedimentary basins that compose the western third of Madagascar (where Lembetabe is located) and where the crustal thickness is about 30 ± 5 km (Andriampenomanana et al., 2017), we used the density and elastic structure from PREM (Dziewonski et Anderson, 1981), and three parameters are varied for the viscosity structure: upper-mantle viscosity (3–5 × 10^{20} Pa.s), lower-mantle viscosity (3–40 × 10^{21} Pa.s), and elastic thickness of the lithosphere (71–96 km). As ice model, the ICE-6G reconstruction (Peltier et al., 2015) is used for the last deglaciation and scaled to the foraminifera isotope-based eustatic curve by Waelbroeck et al. (2002) prior to the LGM, modified as in Dyer et al. (2021). To explore the uncertainty associated with this deglacial timing, GIA simulations are run with two eustatic sea-level curves. For one curve, we set the MIS 6 maximum at 136.5 ka, while we assumed it occurred at 143 ka for the second curve. Further, the absolute and relative sizes of MIS 6 ice sheets are uncertain, which affects LIG sea level (Dendy et al., 2017; Rohling et al., 2017). We therefore vary the size of the Fennoscandian and Laurentide ice sheets during MIS 6 ranging from a large Laurentide and small Fennoscandian ice sheet (as in ICE-6G) to a small Laurentide and large Fennoscandian ice sheet (as in Colleoni et al., 2016) with four intermediate configurations inbetween. Lastly, in order to investigate deviations relative to present day sea level, we set the excess eustatic sea level during the LIG (assumed to last from 129 to 118 ka) to 0 m. Varying both Earth and ice history leads to 576 different GIA predictions. To calculate the probabilistic distribution in time and space of the RSL corrected for GIA, we implemented a Monte-Carlo approach (1 million permutations), as described in Rovere (2022) (https://doi.org/10.5281/zenodo.7231482).

3. Results

3.1. Dating and elevation

Among the 25 *in situ* samples collected on the Lembetabe reef section (Figs. 2), 16 were 100% aragonite or contained less than 1% calcite and were suitable for dating with the uranium-thorium disequilibrium method. The resulting ages fall between 115.0 ± 0.4 ka and 139.0 ± 0.5 ka (Table 1). The back-calculated initial $\delta^{234}U_i$ range falls between 138.0 ± 0.5‰ and 161.2 ± 0.6‰ (Table 1, Fig. 3). The sample IT-19-56 has an initial $\delta^{234}U_i$ of 161.2 ± 0.6 (Fig. 3), which is higher than the value reported by Andersen et al. (2010) for the modern, open ocean seawater (i.e. 144.9 ± 0.4‰ when corrected for analytical biases, see Chutcharavan et al., 2018) and the value for modern coral (145.0 ± 1.5‰, Chutcharavan et al., 2018). Although no calcite was measured with X-ray diffraction, such shift from the modern marine value indicates diagenetic alteration and that ages obtained are unreliable. Higher initial ratio [^{234}U/^{238}U] than the seawater value indicates diagenetic processes that might imply addition of ^{234}U that would produce an older age (we obtained ages of 139 ± 0.5 ka, significantly older than the age range of all others samples). Excluding this sample, the U-series ages on the Lembetabe section fall between 115.0 ± 0.4 ka and 129.5 ± 0.5 ka and the initial $\delta^{234}U_i$ range is reduced, with an average of 145.9 ± 9.1‰ (2SD) (Table 1). The initial δ^{234}U of this smaller dataset appears homogeneous and in good agreement with marine value (Andersen et al., 2010; Chutcharavan et al., 2018).

Most of the samples have high ^{230}Th/^{232}Th activity ratios implying low ^{232}Th concentrations (Table 1) and hence little evidence of any inherited ^{230}Th. However, a few other samples have higher concentrations of ^{232}Th than typical concentrations for surface corals (Shen et al., 2008). Nevertheless, there is no need to correct for detrital thorium since such correction is negligible compared to the analytical error for corals of several thousand years (e.g. Edwards et al., 2003).

As the 15 remaining samples are pristine according to the most rigorous mineralogical criteria and have mutually agreeing initial uranium ratios, this likely precludes any open-system behavior. Therefore, we conclude that our U–Th age results are accurate, and indicate that the development of the fossil reef of Lembetabe is associated with the LIG and that it falls in the 115–129 ka range of the LIG stage (Stirling et al., 1998).

Within the fossil reef, *in situ* corals dated to the LIG were found at elevations ranging between 1.46 ± 0.24 m and 2.20 ± 0.24 m above mean sea level (amsl) (Table 2, see Fig. 2 for location). On average, the fossil reef stands at an elevation of 1.86 ± 0.56 m amsl (Table 2). Regarding the relic shore platform, GPS measurements indicate that the paleo-shoreline (i.e limit between the paleo-beach and the paleo-platform) stands at 2.68 ± 0.10 m amsl (Fig. 6). All the elevations measured with dGNSS in Lembetabe are available in Boyden et Rovere (2021) (https://doi.org/10.5281/zenodo.5727117).

3.2. Paleo RSL

Fossil specimens of corals growing within narrow environmental ranges, such as *Acropora Palmata* were initially considered as relatively accurate sea-level indicators (due to its shallow 1–5 m range of waterdepth, e.g. Lighty et al., 1982; Toscano and et Macintyre, 2003). However, several studies have demonstrated that *Acropora Palmata* can live at greater depth than 5 m (Hubbard, 2009; Zimmer et al., 2006; Bard et al., 2016) and today we know that most coral species are "depth-generalists", and can thus be found over a wide vertical range (Veron, 1995; Carpenter et al., 2008).

As the paleo ecology of a single coral genus does not provide precise sea level information (Hibbert et al., 2016), we aimed to estimate the probable depth range of the fossil reef by analyzing the water depth range of the fossil coral assemblage we discovered. We used global databases from Hibbert et al. (2016) (based on dated fossil corals and depth distribution compiled by the International

Table 1
U–Th ages of corals from Lembetabe. Values in parentheses are $\pm 2\sigma$ absolute uncertainties. Square brackets denote activity ratios. Decay constants are 9.1705×10^{-6} yr^{-1} for ^{230}Th, 2.8221×10^{-6} yr^{-1} for ^{234}U Cheng et al. (2013), and 1.55125×10^{-10} yr^{-1} for ^{238}U Jaffey et al. (1971). Ages are reported relative to the year of analysis, 2019 (for IT-19-23 and IT-19-24) and 2021 (for all others samples), and do not include uncertainties associated with decay constants.

Sample ID	^{238}U (ppb)	^{232}Th (ppt)	^{230}Th (ppt)	[^{234}U/^{238}U]	[^{230}Th/^{238}U]	[^{230}Th/^{232}Th]	Age (ka)	$\delta^{234}U_i$ ‰
IT-19-23	3025.8 (5.9)	60.6 (0.3)	38.4 (0.1)	1.103 (0.002)	0.777 (0.002)	118515 (665)	129.0 (0.7)	147.8 (0.4)
IT-19-24	3160.3 (6.0)	3154.1 (7.0)	39.2 (0.1)	1.103 (0.002)	0.758 (0.002)	2322 (7)	123.4 (0.6)	146.2 (0.3)
IT-19-53	3204.2 (9.3)	30.5 (0.1)	39.6 (0.1)	1.097 (0.003)	0.757 (0.003)	244219 (1065)	124.2 (0.5)	138.0 (0.5)
IT-19-54	2499.9 (7.0)	258.2 (0.5)	30.0 (0.1)	1.110 (0.003)	0.734 (0.002)	21827 (55)	115.0 (0.4)	152.2 (0.6)
IT-19-56[a]	3959.1 (11.2)	125.5 (0.3)	52.6 (0.1)	1.109 (0.003)	0.813 (0.003)	78332 (215)	139.0 (0.5)	161.2 (0.6)
IT-19-57	3033.3 (8.2)	1720.7 (3.1)	38.4 (0.1)	1.100 (0.003)	0.774 (0.002)	4181 (10)	128.7 (0.5)	143.8 (0.5)
IT-19-58	2637.7 (7.6)	739.5 (1.4)	32.6 (0.1)	1.099 (0.003)	0.757 (0.003)	8280 (21)	123.9 (0.4)	141.0 (0.5)
IT-19-60	2719.3 (8.2)	304.4 (0.6)	32.8 (0.1)	1.101 (0.003)	0.738 (0.003)	20209 (50)	118.0 (0.4)	141.0 (0.6)
IT-19-61	2657.3 (7.4)	74.6 (0.2)	33.8 (0.1)	1.104 (0.003)	0.778 (0.002)	85030 (244)	129.2 (0.5)	149.2 (0.6)
IT-19-62	2685.5 (7.7)	1256.9 (2.4)	33.8 (0.1)	1.104 (0.003)	0.770 (0.003)	5039 (13)	126.7 (0.5)	148.1 (0.6)
IT-19-63	2728.1 (7.4)	76.9 (0.2)	34.0 (0.1)	1.100 (0.003)	0.762 (0.002)	82948 (225)	125.3 (0.5)	143.0 (0.5)
IT-19-64	4071.4 (10.8)	486.0 (0.9)	52.0 (0.1)	1.107 (0.003)	0.781 (0.002)	20063 (49)	129.5 (0.5)	153.8 (0.5)
IT-19-65	3217.3 (9.0)	3381.6 (6.1)	40.1 (0.1)	1.099 (0.003)	0.763 (0.002)	2225 (5)	125.9 (0.4)	140.9 (0.5)
IT-19-68[b]	2803.7 (8.3)	256.1 (0.5)	35.4 (0.1)	1.102 (0.003)	0.771 (0.003)	25814 (66)	127.5 (0.5)	146.9 (0.6)
IT-19-70	2635.9 (8.0)	21.7 (0.1)	33.1 (0.1)	1.102 (0.003)	0.768 (0.003)	285236 (1434)	126.4 (0.5)	145.9 (0.6)
IT-19-71	2921.9 (8.1)	39.3 (0.1)	36.7 (0.1)	1.105 (0.003)	0.769 (0.002)	174716 (646)	125.9 (0.4)	150.4 (0.5)

[a] Sample with $\delta^{234}U_i$ indicating open-system behavior.
[b] Sample for which data have been recently published in companion paper (Boyden et al., 2022).

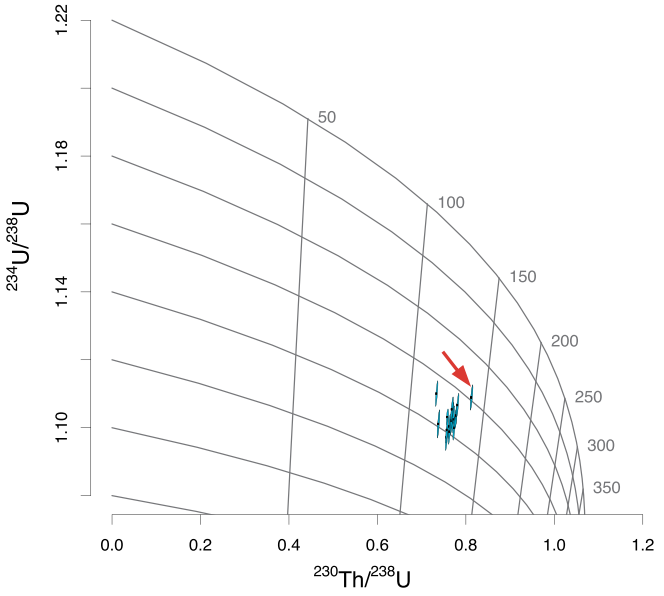

Fig. 3. Distribution of the activity ratios ^{234}U/^{238}U and ^{230}Th/^{238}U measured (on MC-ICPMS NEPTUNE PLUS) for the 16 corals dated from the reef section (using Isoplot-R, option U-Series/evolution and KDE, Vermeesch, 2018). Red arrow: sample IT-19-56 for which initial $\delta^{234}U_i$ is higher than the sea water value (Andersen et al., 2010; Chutcharavan et al., 2018) which yields to an erroneously old age.

Union for the Conservation of Nature - IUCN) and from the Ocean Biodiversity Information System (OBIS) to determine the living depth range of each coral genera/species dated (Table 2). We were able to reduce the probable depth range of the fossil reef to 10–15 m thanks to a few genera/species which are most commonly found living within this depth range (i.e *Acropora*, *Dipsastraea gr. pallida*, *Favites*, and *Platygyra*, Table 2). Using the median depth, the paleo-depth is even reduced to less than 5 m (Table 2). As well, a shallow environnement is suggested from the OBIS database with a few genera/species particularly abundant between 0 and 10 m (i.e *Plesiastrea*, *Dipsastraea*, and *Favites*, Table 2). Finally, the *Pocillopora* sample IT-19-68 exhibits sturdy branches that appear to be flattened, further supporting the hypothesis of a shallow environment well exposed to swells and waves. Hence, despite remaining uncertainties on coral identification at the species level, we conclude that there is a high probability that the fossil coral assemblage is consistent with a shallow environment, likely less than 5 m deep.

As described in our companion paper (Boyden et al., 2022), we interpret the emerged fossil reef as a coral-dominated shallow-water reef sequence, similar to that found in the modern reef flat. To quantify the paleo RSL associated with the fossil reef, we turn to modern analogs for the paleo facies observed in the field, calculating their indicative meaning. The concept of indicative meaning, in paleo sea-level research, indicates the quantification of paleo RSL via a known relationship between a sea-level indicator and a tidal level, such as mean sea level (Van de Plassche, 1982; Shennan et al., 2015). To quantify the indicative meaning, we turn to the modern shallow reef flat facing the fossil one. By using satellite-derived bathymetry (Fig. 4 a, b), we calculate the depth distribution of the backreef. Despite an asymmetrical distribution of the depth frequency (see inset in Fig. 4 c), we calculated a weighted-mean depth of −1.55 m with a variance of 1.31 m. These are used, respectively, as reference water level (RWL) and half of the indicative range (IR), that are then employed in paleo RSL calculations.

We subtracted the RWL from the elevation of the paleo reef (average elevation of all corals that is 1.86 ± 0.56 m amsl, Table 2) and calculate that the paleo RSL associated with this reef is 3.4 ± 1.4 m amsl (Table 2 and Fig. 5). This result is consistent with the paleo RSL obtained with the second indicator surveyed in the area of Lembetabe, i.e., the fossil shore platform. Indeed, the elevation of the paleo-shoreline at 2.68 ± 0.10 m amsl corresponds to the difference in elevation between the paleo-erosional surface and its modern analog (the modern shore platform) (Fig. 6). The agreement between the two independent paleo RSL estimates strengthens our assumption of a shallow environment for the paleo reef we studied. Of note, the discrepancy with the lower paleo RSL inferred from the paleo platform (2.68 ± 0.10 m amsl, in contrast to the higher paleo RSL of 3.4 ± 1.4 m amsl inferred from the fossil reef) suggests a regression in sea level during the late MIS5, following the highstand recorded by the fossil reef. This regression provided the opportunity to form the paleo beach.

Table 2
Elevations for RSL index points, i.e LIG corals. For each coral sample taken from the fossil reef (FR) flat at Lembetabe, we show the calculated paleo-RSL (PRSL). Coral genus (and species whenever possible) was determined using the taxonomic classification of Veron (2000) with modifications by Huang et al. (2014b,a, 2016). When available, depth range and median depth for each coral genus encountered within the fossil reef are indicated. These are taken from the summary of empirically-derived global depth distributions in the fossil coral database from Hibbert et al. (2016). Coral abundance (in percentage) between 0 and 10 m of depth extracted from OBIS database https://obis.org/(Fig. S6). Such values are not used to calculate paleo RSL in this study, and are shown here only as reference. The reference water level (RWL) corresponds to the weighted-mean of the modern reef flat depth. Values in parentheses are $\pm 1\sigma$ values corresponding to half of the indicative range (associated to RWL) and paleo RSL uncertainty (associated to PRSL).

Sample ID	Elevation	Coral genus/species	Depth range	Median Depth	Coral abundance	RWL	PRSL (m)
	(m)		**95% confidence (m)**	**95% confidence (m)**	**between 0–10 m**	**(m)**	**(m)**
IT-19-23	2.13 (0.27)	*Plesiastrea versipora*[a]	- 2 to - 43.7	- 5	79%		
IT-19-24	2.17 (0.27)	*Astreopora listeri or myriophthalma*[a]	0 to - 46	- 34	71% - 25%		
IT-19-53	2.10 (0.24)	*Hydnophora microconos*	0 to - 46.2	- 2	44%		
IT-19-54	1.81 (0.24)	*Dipsastraea gr. pallida*[c]			70% - 18% - 87%		
IT-19-56	1.46 (0.24)	*Acropora*	0 to - 18	- 2.4	71%		
IT-19-57	1.99 (0.24)	*Pocillopora*	0 to - 49	0	55%		
IT-19-58	2.20 (0.24)	*Favites gr. abdita*[a,d]	0 to −17.6	- 4	93% - 94%		
IT-19-60	1.94 (0.24)	*Goniastrea favulus?*[a]	0 to - 46	- 5	93%		
IT-19-61	1.69 (0.24)	*Favites or Acanthastrea*			93% or 59%		
IT-19-62	1.77 (0.24)	*Pocillopora eydouxi*[a]*or verrucosa*	0 to - 49	0	55% - 36%		
IT-19-63	1.75 (0.24)	*Favites*	0 to −17.6	- 4	93%		
IT-19-64	1.27 (0.24)	*Acropora*	0 to - 18	- 2.4	71%		
IT-19-65	2.12 (0.24)	*Pocillopora*	0 to - 64	0	43%		
IT-19-68	2.06 (0.24)	*Pocillopora eydouxi?*[a]	0 to - 49	0	–		
IT-19-70	1.49 (0.24)	*Platygyra daedalea or lamellina*[b]	0 to - 10.1	- 4.5	71% - 75%		
IT-19-71	1.73 (0.24)	*Acanthastrea*			59%		
Mean FR elevation	1.86 (0.56)					−1.5541 (1.3068)	**3.41 (1.43)**

[a] Corals genera for which there is no information at the species level in Hibbert et al., 2016 or OBIS.
[b] For the genus Platygyra, information are given for the species lamellina as no information are available for the species daedalea (Hibbert et al., 2016).
[c] *Dipastraea gr. pallida* includes *D. pallida*, *D. matthai*, and *D. speciosa*.
[d] *Favites gr. abdita* includes *F. abdita* and *F. halicora*.

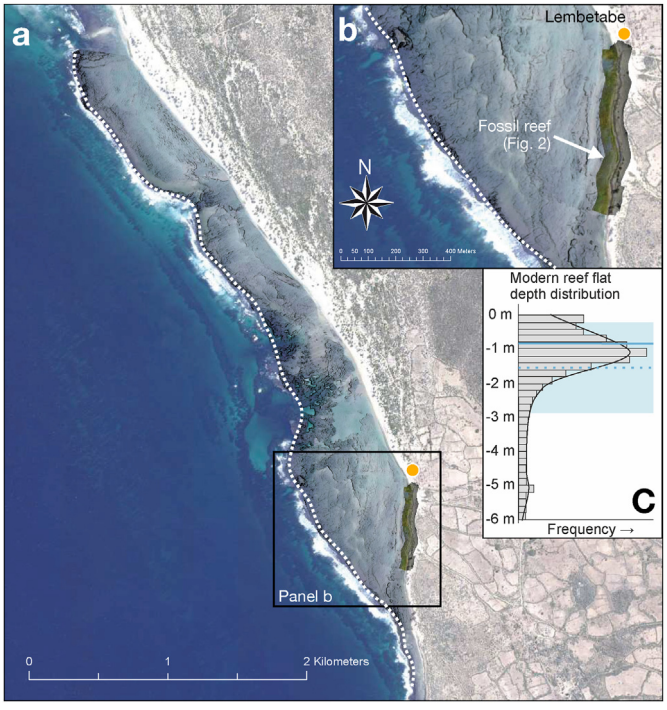

Fig. 4. Modern reef satellite derived bathymetry (see the methods section for details), shown here as hillshadeover a Worldview-2 pansharpened image, ©DigitalGlobe inc. a) entire scene, b) detail close to Lembetabe, with the location of drone-derived data shown in Fig. 2 c) histogram and KDE plot of fringing reef flat depth distribution. Solid blue line represents the median and the dotted blue line represents the mean of the distribution. The shaded area represents the 2σ range around the mean depth (dotted bue line).

3.3. Glacial isostatic adjustment

GIA driven sea-level peaks early in the deglaciation and subsequently decreases due to continental levering and ocean syphoning (Fig. 7 b). GIA models with a fast deglaciation (those with an MIS 6 maximum at 136.5 ka) generally lead to a higher sea level than those with a slower deglaciation. Note that the modeled interglacial ends at 118 ka, which drives the steep drop-off of sea level after this time. We therefore used the GIA correction at 118 ka for data younger than 118 ka.

This prediction does not include excess (i.e. more than present) ice melt. Accounting for the gravitational and deformational effects leads to a GIA or fingerprint signal associated with this excess melt (Hay et al., 2014). For 1 m of sudden ice melt from the West Antarctic Ice Sheet, RSL in Lembetabe would be expected to rise by 1.24 m. Similarly, 1 m of sudden melting from the Greenland Ice Sheet would be recorded as 1.14 m of local sea-level change. Note that these estimates are reduced if melting occurs over a longer time.

4. Discussion

Previous studies dated the fossil reef of Lembetabe to 85 ± 5 kyr BP (Battistini et al., 1976), which corresponds to MIS 5a (Fig. S7). The range of new U–Th ages presented in this study (excluding the oldest sample IT-19-56 with too high initial $\delta^{234}U_i$, Table 1), between 115.0 ± 0.4 ka and 129.5 ± 0.5 ka, falls in the usual LIG timeframe (Stirling et al., 1998) and most of the ages (about 65%, Table 1) belong to the major period of reef building between 121 kyr and 128 kyr highlighted by several studies (e.g. Stirling et al., 1998).

One reason to explain why René Battistini obtained a younger age is that the alpha-counting technique used to measure U–Th disequilibrium is less accurate than modern spectrometry (e.g. Edwards et al., 2003). Another reason might be a lack of a rigorous mineralogical analysis of the collected samples in the laboratory (that could have revealed postmortem diagenetic alteration). Finally, according to sea-level reconstructions, GMSL was about 10 m–20 m below the modern sea level during MIS 5a (Waelbroeck

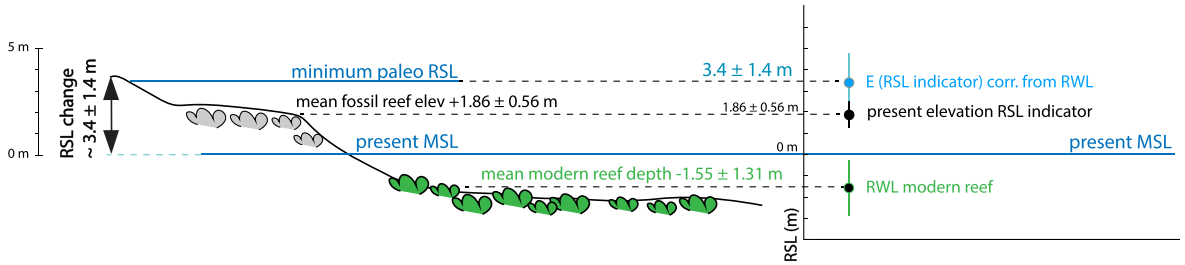

Fig. 5. Paleo RSL calculation from the fossil reef used as a sea-level proxy in Lembetabe (following the methodology of Rovere et al., 2016a). Schematic illustration of our calculation using the fossil reef (FR) and modern reef (MR). MSL: mean sea level. RWL: reference water level.

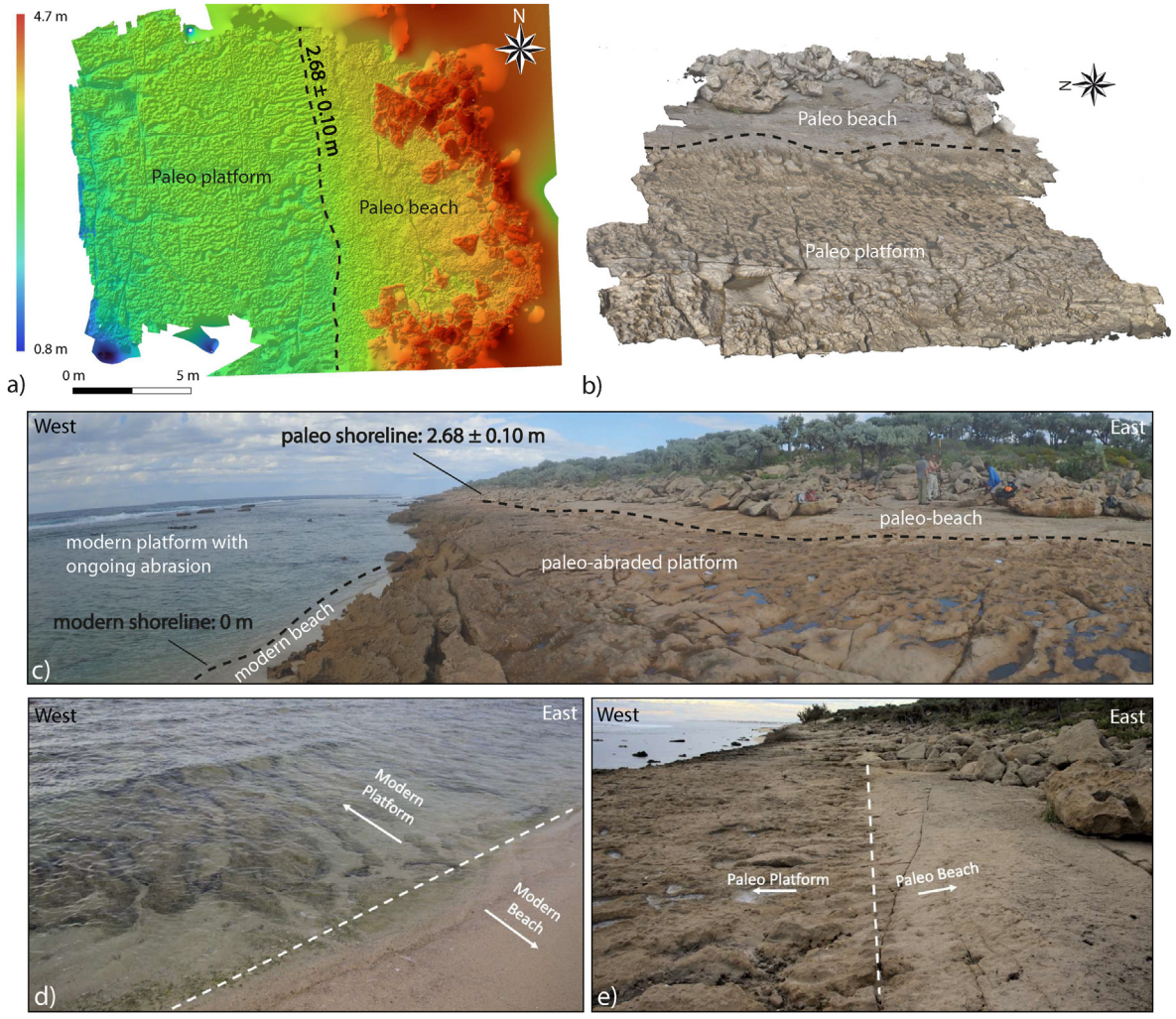

Fig. 6. Paleo RSL calculation in Lembetabe (following the methodology of Rovere et al., 2016a, 2016b) using the paleo shore platform as a second paleo-RSL indicator. a) Digital elevation model (DEM) and b) Orthomosaic image of the relic shore (obtained by photogrammetry and dGNSS ground control points). Dashed black line: limit between the paleo beach and the paleo abraded platform. From the DEM, elevation of the paleo shoreline is inferred at 2.68 ± 0.10 m amsl. c) d) and e) Field pictures of the relic shore and modern shore with decimeter scale furrows. Dashed black and white lines: paleo and modern shorelines.

et al., 2002; Shakun et al., 2015) and direct observations of former sea levels of that vintage are generally restricted to uplifting coastlines. A paleo sea level dated to MIS 5a at about 2 m amsl at Lembetabe would imply substantial uplift, which is inconsistent with the long-term topography of the low coastal area overhanged by the Mahalafy plateau.

Of note is that the interplay between GIA and GMSL changes resulted in a quasi-stable RSL at Lembetabe (Fig. 7 a), as highlighted by field data. The thinness of the fossil reef (about 2 m) and the presence of corals of different ages around the same elevation suggests a prograding reef growing below a stable sea level. These observations are inconsistent with the significant meter-scale sea-level fluctuations proposed during the LIG, which have been estimated to range from 4 m to 15 m according to Kopp et al. (2013) and Rohling et al. (2019). While it is possible to consider occasional drops in sea level within the thickness of the reef (as indicated by

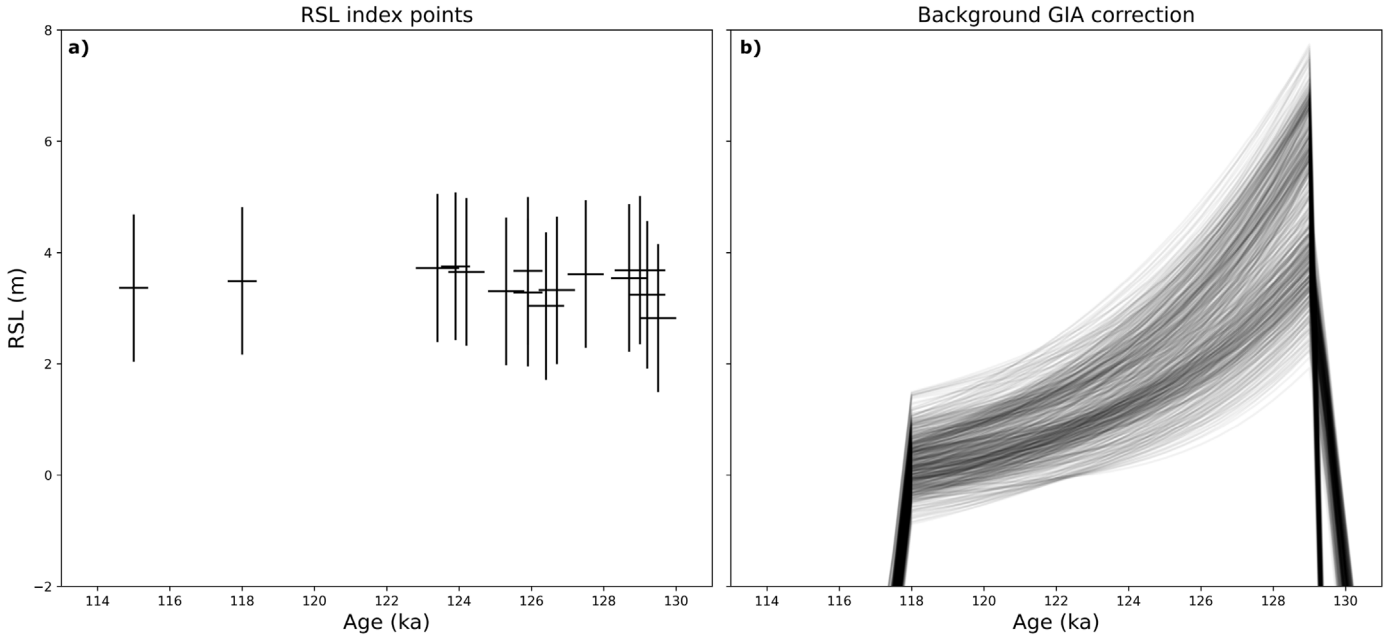

Fig. 7. RSL data (fossil reef) and GIA signal at Lembetabe. a) Sea-level index points and associated ages, as reported in Tables 1 and 2. b) Background GIA signal for Lembetabe (calculated from 576 models), which we consider here to be the amount of sea level change during the interglacial that is purely driven by GIA (i.e. global mean sea level during the last interglacial is set to zero in these calculations). In other words, any difference between the data in a) and the predictions of interglacial sea level in b) must be driven by global mean sea level change.

episodic reef growth patterns observed in the Seychelles, Vyverberg et al., 2018), the presence of paleo-furrows along the terrace, which we associate with the LIG, suggests a prolonged period of stable sea level. These furrows, developed in strongly lithified calcarenite, indicate a sea level that remained constant long enough to form decimeter-scale features (Boyden et al., 2022). Additionally, the flatness of both the paleo and present platforms provides further evidence of a relatively stable sea level, at least since the mid-Holocene highstand for the present platform.

As shown in Fig. 7, RSL proxies and GIA models show, respectively, a linear and a decreasing pattern throughout the LIG. To reconcile such pattern, we show in Fig. 8 the probabilistic distribution in time and space of the RSL corrected for GIA, i.e., subtracting the background GIA from the paleo RSL obtained from dated corals. This provides a first approximation of GMSL, in absence of other significant post-depositional movements and prior to accounting for the fingerprint of ice sheet melting. Our data show that peak LIG RSL in Lembetabe was reached between ca. 118 ka and 115 ka, and was 3.2 m above present (value bounded by 25th and 75th percentiles of, respectively, 2.2 and 4.2 m, Fig. 8).

However, even after correcting our data for GIA, there are several processes that might affect the sea-level estimate from Lembetabe. Some of these remain difficult to quantify, due to lack of independent data or large uncertainties in modeling, as discussed in the sections below.

4.1. Post-depositional erosion

The first potential bias on our calculated RSL may be that the indicators we measured do not represent the original reef surface: part of the fossil reef platform might have been eroded down by karst dissolution. According to available literature, erosion rates on reef limestones range from 0.011 m/kyr to 0.75 m/kyr (e.g. Trudgill, 1979; Viles and et Trudgill, 1984; Opdyke et al., 1984; Spencer, 1985; Paulay and et McEdward, 1990). These rates would imply a removal from 1.5 m to 90 m of reef since the LIG. However, most of these

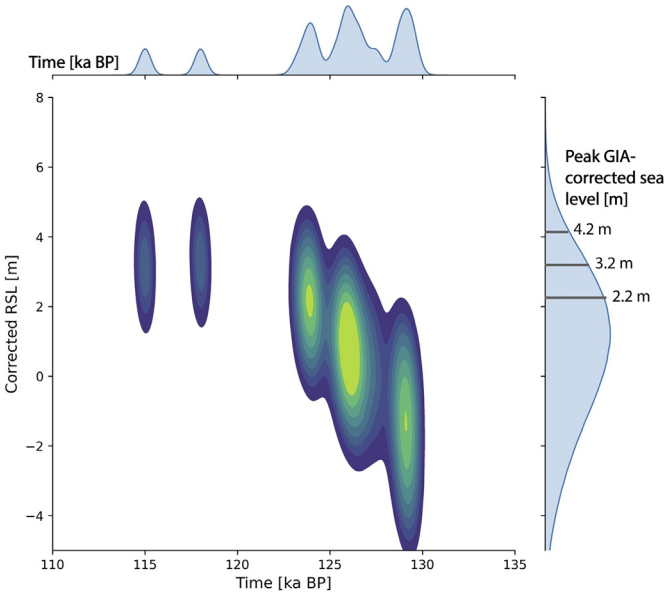

Fig. 8. Kernel density estimate showing the probability density distribution in time and space of RSL at Lembetabe, corrected for GIA. The colorscale is related to the probability density, with a lower probability for darker areas and a higher probability for yellow areas. Graph above the main plot: distribution of ages within the datapoints, including age uncertainties (scale is in ka). Graph on the right side: probability distribution of the RSL through time (scale is in meters). The values show the 25th, 50th and 75th percentiles of the KDE distribution for peak GIA-corrected RSL data.

rates were calculated for areas subject to equatorial to subtropical climate, with important rainfall regimes. Contrary to these locations, the southwestern part of Madagascar is subject to a sahelian to semi-desert climate (Jenkins, 1987).

By using monthly rainfall data from the Global Historical Climatology Network, Dewar et Richard (2007) calculated that the

mean annual rainfall for Toliara (about 160 km north of Lembetabe, along the same coast) is 386 mm/yr. This value is small compared to the mean annual rainfall in intertropical areas, which varies in average between about 1000 mm/yr and 4000 mm/yr (Xie and et Arkin, 1997; Purdy et Winterer, 2001).

Although rainfall is not the only parameter that controls erosion rates on limestones, less rainfall implies lower subaerial erosion rates. This is highlighted by the difference in annual rainfall between the northern and southern Marshall Islands (average rate of 0.33 m/kyr for the Majuro Atoll subject to about 3500 mm/yr of annual rainfall, against 0.12 m/kyr for Enewetak Atoll where rainfall rate is about 1500 mm/yr; Anthony et al., 1989; Purdy and et Winterer, 2001). Also, since the entire reef section at Lembetabe has likely been covered by eolianites following the LIG (Boyden et al., 2022), the now-outcropping small section of fossil reef studied here was protected from erosion until the eolianites were eroded, after the Last Glacial Maximum. Based on the above reasoning, we surmise that the amount of removed reef due to subaerial erosion is negligible. As well, the decimeter scale furrows (about 10–20 cm deep) within the modern platform have almost disappeared within the paleo platform, which suggests that subaerial erosion undergone by the paleo platform is small and negligible compared to the error on our GMSL estimate.

4.2. Tectonics and dynamic topography

Most of Madagascar is considered tectonically stable since the Late Tertiary (e.g. Besairie et al., 1973; Arthaud et al., 1990). Despite this, there is evidence of Quaternary tectonic activity. Through fault mapping and microtectonic analysis, several authors highlighted the presence of active normal faulting in Madagascar (e.g. Arthaud et al., 1990). In Central Madagascar, Kusky et al. (2010) gathered geomorphological and sedimentary evidence of active extensive tectonics. Rindraharisaona et al. (2013) surmised that the moderate seismicity of Madagascar is related to already known active faults that accommodate an E-W extension. In northern Madagascar, Battistini (1965b) discussed active regional tectonics to explain elevations and tilting of a flight of Quaternary emerged marine terraces. The tilting was later attributed to mantle dynamic topography (Stephenson et al., 2019). However, due to the lack of data and the small number of seismic stations, active faults are not well identified outside the center of the island (Rindraharisaona et al., 2013).

Concerning the southwest Malagasian coast, where our study area is situated, it is positioned on the hanging wall of the north-south trending Toliara normal fault, which tends to lower the coastal area and to uplift the inland Mahafaly Plateau region. The deformation related to motion along such crustal fault is limited within a radius similar to the fault depth (at most tens of kilometers) (King et al., 1988), which includes the whole coastal plain since the fault crosses that area with a maximum distance of 15 km from the shoreline. André et al. (2005) investigated the neotectonic deformation of the southern part of Madagascar by analysing facturation of the Eocene limestone of the Mahalafy Plateau to better understand karst genesis and its regional evolution. They concluded that the fracturing at multiple spatial scales is controlled by major regional crustal faults including the Toliara fault, which is the major tectonic feature in the area. Thus the activity of the Toliara fault, although no major earthquake has been reported in the last century, might have had some influence on the present landscape.

Coastal subsidence at a rate of 0.16 mm/yr was suggested to explain two LIG corals found at 13 m below modern SL in drill cores of the Toliara modern barrier reef (Camoin et al., 2004). However, the lack of geomorphologic context for these corals within a broader reef structure, along with the presence of Holocene samples below the two LIG samples, suggest that the LIG corals are not *in situ*. Furthermore, applied to our dataset, this subsidence rate would imply an LIG peak sea level of 24 m, which is inconsistent with ice constraints and the higher end of LIG GMSL estimates (Dutton et al., 2015a, 2015b). To remain within the "classic" LIG GMSL estimate (i.e., 5–10 m above present; Gulev et al., 2021), our location (LIG peak sea level = 3.2 m) would have to be subsiding (since 125 ka) at a much lower rate, between −0.014 and −0.05 mm/yr. Taking into account, instead, the GMSL estimate of Dyer et al. (2021) (i.e 1.2–5.3 m above present), the tectonic vertical land motions would entail uplift (0.016 mm/yr) or slight subsidence (−0.017 mm/yr). However, we remark that these rates are (obviously) not independent from the LIG sea-level record and should be then used with caution.

As the rates mentioned above are based on the modern elevation of the LIG sea-level indicators, they might also include the effects of mantle dynamic topography (DT), which is the vertical crustal motion driven by mantle flow. In the northern tip of Madagascar, Stephenson et al. (2019) studied a set of emerged Pleistocene terraces (including the LIG terrace), standing at various elevations over a distance of at most 80 km. By using geophysical data including a seismic tomography model, they suggested an asthenospheric anomaly (about 125 km deep) for the origin of the spatial gradient of uplift observed. The models of Stephenson et al. (2019) show DT-driven uplift also for the SW part of Madagascar. DT simulations by Austermann et al. (2017) predict 1.96 ± 1.4 m (1σ) of uplift since the LIG at Lembetabe.

One independent constraint on net vertical land motion (including tectonics and DT) at Lembetabe may be derived from the MIS 11 coral rubble unit described by Boyden et al. (2022). In this calcarenite unit that outcrops beneath the MIS 5e units, reaching up to 2.8 m amsl, several coral clasts with a sub-angular shape were discovered. U–Th dating conducted on the samples indicate that these samples likely formed during or after MIS 11 (Boyden et al., 2022). While the preservation of this unit does not allow a detailed facies determination such as the one done for the MIS 5e reef, we might assume that it represents a shallow-water unit, hence we can apply the same indicative meaning to this coral rubble unit, obtaining a first-order estimate of MIS 11 paleo RSL of 4.3 m above present. Using the MIS 11 GMSL estimate of 6–13 m by Raymo and et Mitrovica, 2012 and considering a time interval of 400 ka, this would indicate long-term subsidence rates of −0.004 to −0.02 mm/yr. We remark that these rates must be considered with caution since i) they do not include a quantification of MIS 11 GIA, ii) vertical land motions might not have been constant through time, and iii) the indicative meaning of the MIS 11 coral rubble is tentative and would need more detailed investigation.

5. Conclusion

In this work, we measured and dated a set of sea-level indicators from Lembetabe, in Western Madagascar. We confirmed that the reef developed under higher sea-level conditions during the Last Interglacial, revising its original age attribution to MIS 5e from MIS 5a (Battistini, 1965a)

Coupling a recently published facies description (Boyden et al., 2022) and new satellite-derived bathymetry of the modern reef, we found that the peak paleo RSL at Lembetabe was 3.4 ± 1.4 m above modern sea level. Then, taking into account GIA as calculated by a suite of 576 models with varying mantle viscosity profiles and ice histories, we calculate that GIA-corrected peak LIG sea level in our study area was reached between 118 ka and 115 ka at 3.2 m above present (25th and 75th percentiles of, respectively, 2.2 and 4.2 m). While correcting for vertical land motions carries several

uncertainties and unknowns, independent MIS 11 data seem to indicate a slight subsidence, possibly between −0.004 and −0.02 mm/yr. Applying these rates to our peak sea-level estimate (2.2–4.2 m, reported above), we would obtain a peak LIG sea level between 2.7 and 6.7 m. Overall, this value is in broad agreement with the upper end of the peak LIG sea-level range calculated by Dyer et al. (2021) (1.2–5.3 m) and slightly lower than the one obtained from the Seychelles (7.6 ± 1.7 m, Dutton et al., 2015b). Note, however, that peak sea level in these studies is reported to occur at the beginning of the LIG rather than the end, which is suggested by our data. Our results fall on the low end of the often-cited LIG range (e.g. Dutton et al., 2015a; Gulev et al., 2021, about 5–10 m).

Removing from our peak GMSL estimate the contributions of thermal expansion (0.4 ± 0.1 m, Turney et al., 2020) and mountain glaciers (0.3 ± 0.1 m, Farinotti et al., 2019), the above-mentioned range is further reduced to 2–6 m of sea-level equivalent ice melt from WAIS and GrIS. We remark that this range still does not take into account the melting fingerprint of these two ice caps, which would further lower this estimate.

In conclusion, the fossil reef at Lembetabe, SW Madagascar, represents an excellent site for gauging changes in sea level during the Last Interglacial. Our new field data, radiometric ages and estimates of vertical land motions point to a LIG GMSL slightly lower than hitherto assumed, in line with the recent work of Dyer et al. (2021), and falling at the lower end of the commonly reported LIG peak GMSL. We remark that several aspects related to vertical land motions (in particular, a more precise quantification of the slight subsidence we infer in this study) still need refinement. Tackling these with data independent from the LIG sea-level record remains a priority not only for our study area, but at any location, even in areas commonly considered neotectonically stable as the Malagasian microcontinent.

Credit authors statement

J. Weil-Accardo: Conceptualization, Investigation, Formal analysis, Writing – original draft. P. Boyden: Conceptualization, Investigation, Formal analysis, Writing – review & editing A. Rovere: Conceptualization, Investigation, Methodology, Funding acquisition, Supervision, Project administration, Writing – review & editing N. Godeau: Investigation N. Jaosedy: Investigation A. Guihou: Formal analysis, Writing – review & editing M. Humblet: Formal analysis, Writing – review & editing M. N. Rajaonarivelo: Conceptualization, Supervision J. Austermann: Methodology, Writing – review & editing P. Deschamps: Conceptualization, Investigation, Funding acquisition, Supervision, Project administration, Writing – review & editing.

Declaration of competing interest

The authors declare that they have no known competing financial interests or personal relationships that could have appeared to influence the work reported in this paper.

Data availability

Data are included in the main text and supporting information file as figures. Any additional information (raw GNSS data, SfM-MVS quality reports, and additional visuals from the field) can be found at https://doi.org/10.5281/zenodo.5727117, linked to our companion paper Boyden et al., 2022.

Acknowledgements

We are very grateful to the whole IRD representation of Antananarivo and we deeply thank Claude-Anne Gauthier, Regine Rakotoniaina, IRD drivers Mohamed-Ali and Francois, as well as Mondesir Cromwel for their valuable logistical help. No fieldwork would have been doable without Elahimitogoa Franck Zuma and Mahareta Ramindrisoa who guided us on the field. We also thank chiefs of Lembetabe and Raindrano villages who allowed us to conduct our work in very good conditions. We were hosted at Mamy's place, we deeply thank Mamy, his wife and their adorable family (Ino, Sandrina, Benandru, Mamal … and all their friends) for their care and the time spent together. All on our way, we were lucky to meet great people and we thank them for their smile, help and their kind curiosity. Helene Mariot and Marion Defrance are thanked for their careful maintenance of CEREGE's clean laboratory. The project leading to this publication received funding from two French ANR “Investissement d'avenir” programs through the EQUIPEX ASTER-CEREGE and the DATCARB project from the “Excellente initiative” program of Aix Marseille University A*MIDEX. Funding was also provided by the European Research Council (ERC) under the European Union's Horizon 2020 research and innovation programme (grant agreement n. 802414 to AR) and by the Helmholtz-Exzellenznetzwerke (grant no. ExNet-0001-Phase 2–3) “The Polar System and its Effects on the Ocean Floor (POSY)”. JA acknowledge support from NSF grant OCE-1841888. JWA is supported by a post-doctoral grant of the French National Research Institute for Sustainable Development (IRD).

Appendix U/Th Dating of corals

The chemical and analytical procedures consisting of separating and purifying uranium followed by thorium from the calcium matrix prior to isotope ratio measurements were carried out at CEREGE. The sample is first dissolved with nitric acid. Then, the sample is spiked with a ^{229}Th–^{233}U–^{236}U in-house mixture and allowed to equilibrate. After equilibration, dissolved iron is added to the sample and the pH of the solution is raised to about 8 by adding NH_4OH to coprecipitate uranium and thorium with iron oxy-hydroxides. Uranium and thorium are then separated by extraction chromatography using columns with UTEVA resin. Sample/spike ratios were 8.8 ± 2.3 (1σ) for ^{235}U/^{233}U and 0.21 ± 0.05 (1σ) for ^{230}Th/^{229}Th. For each batch of 11 samples a spiked procedural blank was prepared.

Analyses were conducted on an MC-ICPMS NEPTUNE PLUS following the procedure of Chiang et al. (2019). Briefly, sample solutions diluted in 1% HNO_3 (with traces of HF) were introduced in the mass spectrometer (MS) in dry plasma mode using an Apex Omega HF and a 100 μL/min Opalmist nebulizer. The MS was equipped with a Ni Jet sample cone and a Ni H skimmer cone. The daily sensitivity was about 400 V/ppm for U and Th. The U and Th fractions of each sample were analyzed separately. U fractions were analyzed at about 0.8 V of ^{238}U by peak jumping of ^{233}U, ^{234}U, ^{235}U, ^{236}U on the central SEM equipped with a Retarding Potential Quadrupole (RPQ). Each analysis consisted of 1 block of 600 cycles (which resulted in about 3 mL of sample consumption). Th fractions were analyzed at about 200 kcps of ^{229}Th by peak jumping of ^{229}Th and ^{230}Th on the central SEM equipped with an RPQ. ^{232}Th was monitored on a Faraday cup for each cycle. Each analysis consisted in 1 block of 450 cycles (which resulted in about 2 mL of sample consumption).

For each daily session of analyses (U or Th), abundance sensitivity and hydrides were monitored at mass 237 and 239 on the SEM + RPQ (respectively around 250 ppb and 700 ppb) using a 2 V ^{238}U beam at the beginning and end of each batch. Data were

processed by correcting for SEM dark noise (measured every day), dead time, and on-peak blanks using the Thermo Software. Then, abundance sensitivity, hydrides, peak-jumping beam time-interpolation, instrumental mass bias (for Th, the instrumental mass bias was corrected using multiple analyses of a spiked U SRM960 solution assuming that it is identical for Th and U), contributions from the spike and procedural blanks as well as error propagation were processed using an in-house Microsoft Excel v.16.46 (Microsoft Corporation, Redmond, WA) macro.

Spiked HU-1 processed through the same procedure as the sample was analyzed multiple times to check for accuracy. Average results of HU-1 for this study were: ($^{234}U/^{238}U$) = 0.999 ± 0.001 (2SD, n = 8); ($^{230}Th/^{238}U$) = 1.004 ± 0.002 (2SD, n = 10), in good agreement with published values (Cheng et al., 2013).

Finally, $^{230}Th/^{238}U$ ages were obtained using Isoplot-R (option U-Series/ages) (Vermeesch, 2018).

Supplementary data

Supplementary data to this article can be found online at https://doi.org/10.1016/j.quascirev.2023.108197.

References

Andersen, M., Stirling, C., Zimmermann, B., et Halliday, A., 2010. Precise determination of the open ocean $^{234}U/^{238}U$ composition. G-cubed 11 (12).

André, G., Bergeron, G., et Guyot, L., 2005. Contrôle structural et tectonique sur l'hydrogéologie karstique du plateau Mahafaly (domaine littoral semi-aride, sud-ouest de Madagascar). Karstologia 45 (1), 29–40.

Andriampenomanana, F., Nyblade, A.A., Wysession, M.E., Durrheim, R.J., Tilmann, F., Julià, J., Pratt, M.J., Rambolamanana, G., Aleqabi, G., Shore, P.J., et al., 2017. The structure of the crust and uppermost mantle beneath Madagascar. Geophys. J. Int. 210 (3), 1525–1544.

Anthony, S.S., Peterson, F.L., Mackenzie, F.T., et Hamlin, S.N., 1989. Geohydrology of the Laura fresh-water lens, Majuro atoll: a hydrogeochemical approach. Geol. Soc. Am. Bull. 101 (8), 1066–1075.

Arthaud, F., Grillot, J.-C., et Raunet, M., 1990. La tectonique cassante à Madagascar: son incidence sur la géomorphologie et sur les écoulements. Can. J. Earth Sci. 27 (10), 1394–1407.

Austermann, J., Mitrovica, J.X., Huybers, P., et Rovere, A., 2017. Detection of a dynamic topography signal in Last Interglacial sea-level records. Sci. Adv. 3 (7), e1700457.

Bard, E., Hamelin, B., Deschamps, P., et Camoin, G., 2016. Comment on "Younger Dryas sea level and meltwater pulse 1B recorded in Barbados reefal crest coral *Acropora palmata*" by NA Abdul et al. Paleoceanography 31 (12), 1603–1608.

Bard, E., Hamelin, B., et Fairbanks, R.G., 1990. U-Th ages obtained by mass spectrometry in corals from Barbados: sea level during the past 130,000 years. Nature 346 (6283), 456.

Barlow, N.L., McClymont, E.L., Whitehouse, P.L., Stokes, C.R., Jamieson, S.S., Woodroffe, S.A., Bentley, M.J., Callard, S.L., Cofaigh, C.Ó., Evans, D.J., et al., 2018. Lack of evidence for a substantial sea-level fluctuation within the Last Interglacial. Nat. Geosci. 11 (9), 627–634.

Battistini, R., 1965a. L'extrême-Sud de Madagascar. Thèse de doctorat, California Institute of Technology.

Battistini, R., 1965b. Le Quaternaire littoral de l'extrême Nord de Madagascar. Quaternaire 2 (2), 133–144.

Battistini, R., 1966. Le Quaternaire littoral des environs de Dar-es-Salam (Tanzanie). Quaternaire 3 (3), 191–201.

Battistini, R., 1969. Le Quaternaire du littoral kenyan entre Mombasa et Malindi. Quaternaire 6 (3), 229–238.

Battistini, R., 1970a. Deux datations absolues du haut Flandrien de Fénérive-est (côte orientale de Madagascar). Madagascar Revue de Géographie, pp. 150–161.

Battistini, R., 1970b. Etat des connaissances sur les variations du niveau marin à Madagascar depuis 10.000 ans. Comptes rendus Semaine géologique Madagascar, pp. 13–15.

Battistini, R., 1972. L'hypothèse de l'absence de hauts stationnements marins Quaternaires: essai d'application à Madagascar et au sud-ouest de l'Océan Indien. Quaternaire 9 (2), 75–81.

Battistini, R., 1977. Ages absolus $^{230}Th/^{234}U$ de dépôts marins Pleistocenes à Madagascar et dans les iles voisines. Madagascar Revue de Géographie, pp. 73–86.

Battistini, R., 1984. Mise au point sur la terminologie du Quaternaire malgache. Madagascar Revue de Géographie (45), 9–25.

Battistini, R., et al., 1976. Datation par la méthode $^{230}Th/^{234}U$ du Pleistocene moyen marin de Madagascar et des iles voisines. Comptes rendus Société Géologique Française (5), 201.

Battistini, R., et Cremers, G., 1972. Geomorphology and vegetation of iles glorieuses. Atoll Res. Bull. 159, 1–27.

Battistini, R., Guilcher, A., et Marec, A., 1970. Morphologie et formations Quaternaires du littoral Occidental de Madagascar entre Maintirano et le cap Saint-André. Madagascar Revue de Géographie 16.

Battistini, R., et Jouannic, C., 1979. Recherches sur la géomorphologie de l'atoll Farquhar (archipel des Seychelles). Atoll Res. Bull.

Besairie, H., et al., 1973. Précis de géologie malgache. Annales de géologie de Madagascar, p. 36.

Bilmes, A., D'Elia, L., Lopez, L., Richiano, S., Varela, A., del Pilar Alvarez, M., Bucher, J., Eymard, I., Muravchik, M., Franzese, J., et al., 2019. Digital outcrop modelling using "structure-from-motion" photogrammetry: acquisition strategies, validation and interpretations to different sedimentary environments. J. S. Am. Earth Sci. 96, 102325.

Bistacchi, A., Balsamo, F., Storti, F., Mozafari, M., Swennen, R., Solum, J., Tueckmantel, C., et Taberner, C., 2015. Photogrammetric digital outcrop reconstruction, visualization with textured surfaces, and three-dimensional structural analysis and modeling: innovative methodologies applied to fault-related dolomitization (Vajont Limestone, Southern Alps, Italy). Geosphere 11 (6), 2031–2048.

Blanchon, P., Eisenhauer, A., Fietzke, J., et Liebetrau, V., 2009. Rapid sea-level rise and reef back-stepping at the close of the Last Interglacial highstand. Nature 458 (7240), 881–884.

Boyden, P., et Rovere, A., 2021. Electronic Supplementary Material for "Revisiting Batistini: Pleistocene Coastal Evolution of Southwestern Madagascar" https://doi.org/10.5281/zenodo.5727117.

Boyden, P., Weil-Accardo, J., Deschamps, P., Godeau, N., Jaosedy, N., Guihou, A., Rajaonarivelo, M.N., O'Leary, M., Humblet, M., Rovere, A., et al., 2022. Revisiting Battistini: Pleistocene coastal evolution of southwestern Madagascar. Open Quat. 8 (1), 1–17.

Boyden, P., Weil-Accardo, J., Deschamps, P., Oppo, D., et Rovere, A., 2021. Last interglacial sea-level proxies in east africa and the western Indian ocean. Earth Syst. Sci. Data 13 (4), 1633–1651.

Camoin, G., Montaggioni, L., et Braithwaite, C., 2004. Late glacial to post glacial sea levels in the Western Indian Ocean. Mar. Geol. 206 (1–4), 119–146.

Carpenter, K.E., Abrar, M., Aeby, G., Aronson, R.B., Banks, S., Bruckner, A., Chiriboga, A., Cortés, J., Delbeek, J.C., DeVantier, L., et al., 2008. One-third of reef-building corals face elevated extinction risk from climate change and local impacts. Science 321 (5888), 560–563.

Casella, E., Collin, A., Harris, D., Ferse, S., Bejarano, S., Parravicini, V., Hench, J.L., et Rovere, A., 2017. Mapping coral reefs using consumer-grade drones and structure from motion photogrammetry techniques. Coral Reefs 36 (1), 269–275.

Chappell, J., 1974. Geology of coral terraces, Huon Peninsula, New Guinea: a study of Quaternary tectonic movements and sea-level changes. Geol. Soc. Am. Bull. 85 (4), 553–570.

Cheng, H., Edwards, R.L., Shen, C.-C., Polyak, V.J., Asmerom, Y., Woodhead, J., Hellstrom, J., Wang, Y., Kong, X., Spötl, C., et al., 2013. Improvements in ^{230}Th dating, ^{230}Th and ^{234}U half-life values, and U–Th isotopic measurements by multi-collector inductively coupled plasma mass spectrometry. Earth Planet Sci. Lett. 371, 82–91.

Chiang, H.-W., Lu, Y., Wang, X., Lin, K., et Liu, X., 2019. Optimizing MC-ICP-MS with SEM protocols for determination of U and Th isotope ratios and ^{230}Th ages in carbonates. Quat. Geochronol. 50, 75–90.

Church, J., Clark, P., Cazenave, A., Gregory, J., Jevrejeva, S., Levermann, A., Merrifield, M., Milne, G., Nerem, R., Nunn, P., Payne, A., Pfeffer, W., Stammer, D., et Unnikrishnan, A., 2013. Climate Change 2013: the Physical Science Basis. Contribution of Working Group I to the Fifth Assessment Report of the Intergovernmental Panel on Climate Change.

Chutcharavan, P.M., Dutton, A., et Ellwood, M.J., 2018. Seawater $^{234}U/^{238}U$ recorded by modern and fossil corals. Geochem. Cosmochim. Acta 224, 1–17.

Colleoni, F., Wekerle, C., Näslund, J.-O., Brandefelt, J., et Masina, S., 2016. Constraint on the penultimate glacial maximum Northern Hemisphere ice topography (≈ 140 kyrs BP). Quat. Sci. Rev. 137, 97–112.

Dendy, S., Austermann, J., Creveling, J., et Mitrovica, J., 2017. Sensitivity of Last Interglacial sea-level high stands to ice sheet configuration during Marine Isotope Stage 6. Quat. Sci. Rev. 171, 234–244.

Deschamps, P., Durand, N., Bard, E., Hamelin, B., Camoin, G., Thomas, A.L., Henderson, G.M., Okuno, J., et Yokoyama, Y., 2012. Ice-sheet collapse and sea-level rise at the Bølling warming 14,600 years ago. Nature 483 (7391), 559–564.

Dewar, R.E., et Richard, A.F., 2007. Evolution in the hypervariable environment of Madagascar. Proc. Natl. Acad. Sci. USA 104 (34), 13723–13727.

Dutton, A., Carlson, A.E., Long, A., Milne, G.A., Clark, P.U., DeConto, R., Horton, B.P., Rahmstorf, S., et Raymo, M.E., 2015a. Sea-level rise due to polar ice-sheet mass loss during past warm periods. Science 349 (6244), aaa4019.

Dutton, A., Webster, J.M., Zwartz, D., Lambeck, K., et Wohlfarth, B., 2015b. Tropical tales of polar ice: evidence of Last Interglacial polar ice sheet retreat recorded by fossil reefs of the granitic Seychelles islands. Quat. Sci. Rev. 107, 182–196.

Dyer, B., Austermann, J., D'Andrea, W.J., Creel, R.C., Sandstrom, M.R., Cashman, M., Rovere, A., et Raymo, M.E., 2021. Sea-level trends across the Bahamas constrain peak Last Interglacial ice melt. Proc. Natl. Acad. Sci. USA 118 (33), e2026839118.

Dziewonski, A.M., et Anderson, D.L., 1981. Preliminary reference Earth model. Phys. Earth Planet. In. 25 (4), 297–356.

Edwards, R., Gallup, C.D., et Cheng, H., 2003. Uranium-series dating of marine and lacustrine carbonates. Rev. Mineral. Geochem. 52 (1), 363–405.

Edwards, R.L., 1988. High Precision Thorium-230 Ages of Corals and the Timing of Sea Level Fluctuations in the Late Quaternary. Thèse de doctorat. California

Institute of Technology.
Edwards, R.L., Chen, J., et Wasserburg, G., 1987. ^{238}U - ^{234}U - ^{230}Th - ^{232}Th systematics and the precise measurement of time over the past 500,000 years. Earth Planet Sci. Lett. 81 (2–3), 175–192.
Farinotti, D., Huss, M., Fürst, J.J., Landmann, J., Machguth, H., Maussion, F., et Pandit, A., 2019. A consensus estimate for the ice thickness distribution of all glaciers on Earth. Nat. Geosci. 12 (3), 168–173.
Fox-Kemper, B., Hewitt, H.T., Xiao, C., Aoalgeirsdottir, G., Drijfhout, S.S., Edwards, T.L., Golledge, N.R., Hemer, M., Kopp, R.E., Krinner, G., Mix, A., Notz, D., Nowicki, S., Nurhati, I.S., Ruiz, L., Sallée, J.-B., Slangen, A.B.A., et Yu, Y., 2021. Ocean, Cryosphere and Sea Level Change in Climate Change 2021: the Physical Science Basis. Contribution of Working Group I to the Sixth Assessment Report of the Intergovernmental Panel on Climate Change.
Gregory, J.M., Griffies, S.M., Hughes, C.W., Lowe, J.A., Church, J.A., Fukimori, I., Gomez, N., Kopp, R.E., Landerer, F., Cozannet, G.L., et al., 2019. Concepts and terminology for sea level: mean, variability and change, both local and global. Surv. Geophys. 40 (6), 1251–1289.
Guilcher, A., 1954. Les recifs coralliens du nord-ouest de Madagascar. Bull. Assoc. Geogr. Fr. 31 (245), 147–156.
Gulev, S.K., Thorne, P.W., Ahn, J., Dentener, F.J., Domingues, C.M., Gerland, S., Gong, D., Kaufman, D.S., Nnamchi, H.C., Quaas, J., Rivera, J.A., Sathyendranath, S., Smith, S.L., Trewin, B., von Shuckmann, K., et Vose, R.S., 2021. Changing State of the Climate System in Climate Change 2021: the Physical Science Basis. Contribution of Working Group I to the Sixth Assessment Report of the Intergovernmental Panel on Climate Change.
Hay, C., Mitrovica, J.X., Gomez, N., Creveling, J.R., Austermann, J., et Kopp, R.E., 2014. The sea-level fingerprints of ice-sheet collapse during interglacial periods. Quat. Sci. Rev. 87, 60–69.
Hibbert, F.D., Rohling, E.J., Dutton, A., Williams, F.H., Chutcharavan, P.M., Zhao, C., et Tamisiea, M.E., 2016. Coral indicators of past sea-level change: a global repository of U-series dated benchmarks. Quat. Sci. Rev. 145, 1–56.
Huang, D., Arrigoni, R., Benzoni, F., Fukami, H., Knowlton, N., Smith, N.D., Stolarski, J., Chou, L.M., et Budd, A.F., 2016. Taxonomic classification of the reef coral family *Lobophylliidae* (*Cnidaria: anthozoa: Scleractinia*). Zool. J. Linn. Soc. 178 (3), 436–481.
Huang, D., Benzoni, F., Arrigoni, R., Baird, A.H., Berumen, M.L., Bouwmeester, J., Chou, L.M., Fukami, H., Licuanan, W.Y., Lovell, E.R., et al., 2014a. Towards a phylogenetic classification of reef corals: the indo-pacific genera *merulina, goniastrea* and *scapophyllia* (*scleractinia, merulinidae*). Zool. Scripta 43 (5), 531–548.
Huang, D., Benzoni, F., Fukami, H., Knowlton, N., Smith, N.D., et Budd, A.F., 2014b. Taxonomic classification of the reef coral families *merulinidae, montastraeidae*, and *diploastraeidae* (*Cnidaria: anthozoa: scleractinia*). Zool. J. Linn. Soc. 171 (2), 277–355.
Hubbard, D.K., 2009. Depth-related and Species-Related Patterns of Holocene Reef Accretion in the Caribbean and Western Atlantic: A Critical Assessment of Existing Models. *Perspectives In Carbonate Geology*. A tribute to the career of Robert Nathan Ginsburg, pp. 1–18.
Ivanovich, M., et Harmon, R.S., 1992. Uranium-series disequilibrium: applications to earth, marine, and environmental sciences 2, 019854278x.
Jaffey, A., Flynn, K., Glendenin, L., Bentley, W.t., et Essling, A., 1971. Precision measurement of half-lives and specific activities of ^{235}U and ^{238}U. Phys. Rev. C 4 (5), 1889.
Jenkins, M.D., 1987. Madagascar: an Environmental Profile, 9782880326074.
Kendall, R.A., Mitrovica, J.X., et Milne, G.A., 2005. On post-glacial sea level–ii. numerical formulation and comparative results on spherically symmetric models. Geophys. J. Int. 161 (3), 679–706.
Kerans, C., Zahm, C., Bachtel, S.L., Hearty, P., et Cheng, H., 2019. Anatomy of a late Quaternary carbonate island: constraints on timing and magnitude of sea-level fluctuations, West Caicos, Turks and Caicos Islands, BWI. Quat. Sci. Rev. 205, 193–223.
King, G.C., Stein, R.S., et Rundle, J.B., 1988. The growth of geological structures by repeated earthquakes 1. conceptual framework. J. Geophys. Res. Solid Earth 93 (B11), 13307–13318.
Kopp, R.E., Simons, F.J., Mitrovica, J.X., Maloof, A.C., et Oppenheimer, M., 2013. A probabilistic assessment of sea level variations within the Last Interglacial stage. Geophys. J. Int. 193 (2), 711–716.
Kusky, T.M., Toraman, E., Raharimahefa, T., et Rasoazanamparany, C., 2010. Active tectonics of the Alaotra–Ankay graben system, Madagascar: possible extension of Somalian–African diffusive plate boundary? Gondwana Res. 18 (2–3), 274–294.
Lambeck, K., et Chappell, J., 2001. Sea level change through the last glacial cycle. Science 292 (5517), 679–686.
Lemoine, P., 1906. Etudes géologiques dans le Nord de Madagascar, contributions à l'histoire géologique de l'Océan Indien. Thèse de doctorat, Thése Sciences Paris.
Lighty, R.G., Macintyre, I.G., et Stuckenrath, R., 1982. *Acropora palmata* reef framework: a reliable indicator of sea level in the western Atlantic for the past 10,000 years. Coral Reefs 1 (2), 125–130.
O'Leary, M.J., Hearty, P.J., Thompson, W.G., Raymo, M.E., Mitrovica, J.X., et Webster, J.M., 2013. Ice sheet collapse following a prolonged period of stable sea level during the Last Interglacial. Nat. Geosci. 6 (9), 796–800.
Opdyke, N., Spangler, D., Smith, D., Jones, D., et Lindquist, R., 1984. Origin of the epeirogenic uplift of Pliocene-Pleistocene beach ridges in Florida and development of the Florida karst. Geology 12 (4), 226–228.
Paulay, G., et McEdward, L.R., 1990. A simulation model of island reef morphology: the effects of sea level fluctuations, growth, subsidence and erosion. Coral Reefs 9 (2), 51–62.
Peltier, W.R., Argus, D., et Drummond, R., 2015. Space geodesy constrains ice age terminal deglaciation: the global ICE-6G_C (VM5a) model. J. Geophys. Res. Solid Earth 120 (1), 450–487.
Polyak, V.J., Onac, B.P., Fornós, J.J., Hay, C., Asmerom, Y., Dorale, J.A., Ginés, J., Tuccimei, P., et Ginés, A., 2018. A highly resolved record of relative sea level in the western Mediterranean Sea during the Last Interglacial period. Nat. Geosci. 11 (11), 860–864.
Pörtner, H.-O., Roberts, D.C., Masson-Delmotte, V., Zhai, P., Tignor, M., Poloczanska, E., et Weyer, N., 2019. Intergovernmental Panel on Climate Change Special Report on the Ocean and Cryosphere in a Changing Climate.
Purdy, E.G., et Winterer, E.L., 2001. Origin of atoll lagoons. Geol. Soc. Am. Bull. 113 (7), 837–854.
Raymo, M.E., et Mitrovica, J.X., 2012. Collapse of polar ice sheets during the stage 11 interglacial. Nature 483 (7390), 453–456.
Rindraharisaona, E.J., Guidarelli, M., Aoudia, A., et Rambolamanana, G., 2013. Earth structure and instrumental seismicity of Madagascar: implications on the seismotectonics. Tectonophysics 594, 165–181.
Rohling, E.J., Hibbert, F.D., Grant, K.M., Galaasen, E.V., Irvalı, N., Kleiven, H.F., Marino, G., Ninnemann, U., Roberts, A.P., Rosenthal, Y., et al., 2019. Asynchronous Antarctic and Greenland ice-volume contributions to the Last Interglacial sea-level highstand. Nat. Commun. 10 (1), 1–9.
Rohling, E.J., Hibbert, F.D., Williams, F.H., Grant, K.M., Marino, G., Foster, G.L., Hennekam, R., De Lange, G.J., Roberts, A.P., Yu, J., et al., 2017. Differences between the last two glacial maxima and implications for ice-sheet, $\delta^{18}O$, and sea-level reconstructions. Quat. Sci. Rev. 176, 1–28.
Rovere, A., 2022. Paleo Sea Level Utilities. https://doi.org/10.5281/zenodo.7231482, version 1.6.
Rovere, A., Raymo, M.E., Vacchi, M., Lorscheid, T., Stocchi, P., Gomez-Pujol, L., Harris, D.L., Casella, E., O'Leary, M.J., et Hearty, P.J., 2016a. The analysis of Last Interglacial (MIS 5e) relative sea-level indicators: reconstructing sea-level in a warmer world. Earth Sci. Rev. 159, 404–427.
Rovere, A., Ryan, D.D., Vacchi, M., Dutton, A., Simms, A.R., et Murray-Wallace, C.V., 2022. The world atlas of last interglacial shorelines (version 1.0). Earth Syst. Sci. Data Discuss. 1–37.
Rovere, A., Stocchi, P., et Vacchi, M., 2016b. Eustatic and relative sea level changes. Curr. Clim. Change Rep. 2 (4), 221–231.
Scoffin, T.P., Stoddart, D., et Rosen, B.R., 1978. The nature and significance of microatolls. Philos. Trans. R. Soc. Lond. B Biol. Sci. 284 (999), 99–122.
Sepulcre, S., Durand, N., et Bard, E., 2009. Mineralogical determination of reef and periplatform carbonates: calibration and implications for paleoceanography and radiochronology. Global Planet. Change 66 (1–2), 1–9.
Shackleton, N., et Matthews, R., 1977. Oxygen isotope stratigraphy of Late Pleistocene coral terraces in Barbados. Nature 268 (5621), 618–620.
Shakun, J.D., Lea, D.W., Lisiecki, L.E., et Raymo, M.E., 2015. An 800-kyr record of global surface ocean $\delta^{18}O$ and implications for ice volume-temperature coupling. Earth Planet Sci. Lett. 426, 58–68.
Shen, C.-C., Li, K.-S., Sieh, K., Natawidjaja, D., Cheng, H., Wang, X., Edwards, R.L., Lam, D.D., Hsieh, Y.-T., Fan, T.-Y., et al., 2008. Variation of initial $^{230}Th/^{232}Th$ and limits of high precision U–Th dating of shallow-water corals. Geochem. Cosmochim. Acta 72 (17), 4201–4223.
Shennan, I., Long, A.J., et Horton, B.P., 2015. Handbook of Sea-Level Research: Framing Research Questions, 9781118452585.
Shepherd, A., Ivins, E.R., Barletta, V.R., Bentley, M.J., Bettadpur, S., Briggs, K.H., Bromwich, D.H., Forsberg, R., Galin, N., Horwath, M., et al., 2012. A reconciled estimate of ice-sheet mass balance. Science 338 (6111), 1183–1189.
Sieh, K., Ward, S.N., Natawidjaja, D., et Suwargadi, B.W., 1999. Crustal deformation at the Sumatran subduction zone revealed by coral rings. Geophys. Res. Lett. 26 (20), 3141–3144.
Simms, A.R., Anderson, J.B., DeWitt, R., Lambeck, K., et Purcell, A., 2013. Quantifying rates of coastal subsidence since the Last Interglacial and the role of sediment loading. Global Planet. Change 111, 296–308.
Spencer, T., 1985. Weathering rates on a Caribbean reef limestone: results and implications. Mar. Geol. 69 (1–2), 195–201.
Stephenson, S.N., White, N.J., Li, T., et Robinson, L.F., 2019. Disentangling interglacial sea level and global dynamic topography: analysis of Madagascar. Earth Planet Sci. Lett. 519, 61–69.
Stirling, C., Esat, T., Lambeck, K., et McCulloch, M., 1998. Timing and duration of the Last Interglacial: evidence for a restricted interval of widespread coral reef growth. Earth Planet Sci. Lett. 160 (3–4), 745–762.
Toscano, M.A., et Macintyre, I.G., 2003. Corrected western Atlantic sea-level curve for the last 11,000 years based on calibrated ^{14}C dates from *Acropora palmata* framework and intertidal mangrove peat. Coral Reefs 22 (3), 257–270.
Trudgill, S., 1979. Surface lowering and landform evolution on Aldabra. Philos. Trans. R. Soc. Lond. B Biol. Sci. 286 (1011), 35–45.
Turney, C.S.M., Jones, R.T., McKay, N.P., van Sebille, E., Thomas, Z.A., Hillenbrand, C.-D., et Fogwill, C.J., 2020. A global mean sea surface temperature dataset for the Last Interglacial (129–116 ka) and contribution of thermal expansion to sea level change. Earth Syst. Sci. Data 12 (4), 3341–3356.
Van de Plassche, O., 1982. Sea-level change and water-level movements in The Netherlands during the Holocene. Meded. Rijks Geol. Dienst 36 (1), 1–93.
Veeh, H.H., 1966. $^{230}Th/^{238}U$ and $^{234}U/^{238}U$ ages of Pleistocene high sea level stand. J. Geophys. Res. 71 (14), 3379–3386.
Vermeesch, P., 2018. IsoplotR: a free and open toolbox for geochronology. Geosci.

Front. 9 (5), 1479–1493.
Veron, J.E.N., 1995. Corals in Space and Time: the Biogeography and Evolution of the *Scleractinia*, 0801482631.
Veron, J.E.N., 2000. Corals of the World, 0642322368.
Viles, H., et Trudgill, S., 1984. Long term remeasurements of micro-erosion meter rates, Aldabra Atoll, Indian Ocean. Earth Surf. Process. Landforms 9 (1), 89–94.
Vyverberg, K., Dechnik, B., Dutton, A., Webster, J.M., Zwartz, D., et Portell, R.W., 2018. Episodic reef growth in the granitic Seychelles during the Last Interglacial: implications for polar ice sheet dynamics. Mar. Geol. 399, 170–187.
Waelbroeck, C., Labeyrie, L., Michel, E., Duplessy, J.C., McManus, J., Lambeck, K., Balbon, E., et Labracherie, M., 2002. Sea-level and deep water temperature changes derived from benthic foraminifera isotopic records. Quat. Sci. Rev. 21 (1–3), 295–305.
Xie, P., et Arkin, P.A., 1997. Global precipitation: a 17-year monthly analysis based on gauge observations, satellite estimates, and numerical model outputs. Bull. Am. Meteorol. Soc. 78 (11), 2539–2558.
Zimmer, B., Precht, W., Hickerson, E., et Sinclair, J., 2006. Discovery of *Acropora palmata* at the flower garden banks national marine sanctuary, northwestern Gulf of Mexico. Coral Reefs 25 (2), 192, 192.